



Effect of Post-Annealing on the Phase Transformation and Critical Current Density of (Bi, Pb)-2223/AgAu Tapes

Xiaobo Ma^{1,2} · Shengnan Zhang² · Pingxiang Zhang^{1,2} · Chengshan Li² · Guoqing Liu² · Zeming Yu² · Jinshan Li¹

Received: 26 November 2019 / Accepted: 26 December 2019 / Published online: 10 January 2020
© Springer Science+Business Media, LLC, part of Springer Nature 2020

Abstract

During the sintering process of Ag-alloy sheathed Bi-2223 tapes, post-annealing (PA) played an important role on the final current capacity by forming a Pb-rich phase named $(\text{Pb,Bi})_3\text{Sr}_2\text{Ca}_2\text{CuO}_x$ (3221) and healing the cracks. Due to the different oxygen penetration rate between AgAu alloy and pure Ag, which is traditionally used in other Bi-2223 tapes, the influence of PA parameters on the 3221 phase content, microstructures, and current capacity of AgAu tapes should be systematically studied. In this study, PA processes with different temperatures of 770–800 °C have been performed on fully reacted 37-filamentary (Bi, Pb)-2223/AgAu tapes in the atmosphere of 7.5% O₂ balanced with Ar. It is found that the 3221 phase appeared after PA with its amount first increasing then decreasing with increasing PA temperature. The critical temperature T_c and peak temperature (T_p) obtained with AC susceptibility measurement both increased with increasing PA temperature, and reached the maximum value at 780 °C then decreased with increasing PA temperature. Due to the improvement of T_c and intergrain connectivity, the critical current density (J_c) increased by 24% after PA at 780 °C. Meanwhile, the 3221 phase formation mechanism has also been systematically discussed by varying the amount of remnant liquid in tapes in HT1 process.

Keywords Bi-2223/AgAu tapes · Post-annealing method · Pb-rich phase · Intergrain connectivity

1 Introduction

$\text{Bi}_2\text{Sr}_2\text{Ca}_2\text{Cu}_3\text{O}_{10+\delta}$ (Bi-2223) high temperature superconductors have a high potential for applications in a number of electrical devices such as power transmission cables, transformers, magnets, motors, and generators [1–3]. In order to obtain high performance in Bi-2223 superconducting tapes, much effort has been made [4–8].

AgAu sheathed Bi-2223 tapes with lower thermal and electrical conductivity are a good choice for manufacturing HTS current leads [9]. However, their low critical current density compared with traditional Bi-2223/Ag superconducting tapes [10], as well as the high manufacturing costs, is the major

limiting factors for applications, so it is very necessary to improve critical current density of AgAu sheathed Bi-2223 tapes.

It was well known that the critical current density of Bi-2223 tapes is mainly determined by two aspects highly phase pure Bi-2223 with perfect texture, superior grain connectivity. Bi-2223 phase content can be improved by optimizing precursor powder preparation and tape heat-treatment process [11–13]. While grain connectivity has become a key factor for improving J_c , it is reported that the PA process can enhance the J_c by 10–25% at normal pressure [14, 15] and by 30–40% with high pressure heat treatment [16, 17] in Bi-2223/Ag superconducting tapes through improving inter-grain connectivity. Due to the low oxygen diffusion rate of AgAu sheath comparing with Ag sheath, the influences of post annealing parameters on the Pb-rich phase formation process in AgAu sheath Bi-2223 tape are different from that in Ag sheath tape. Therefore, the post-annealing process of AgAu sheath Bi-2223 tape needs to be systematically optimized; meanwhile, the evolution process of phase composition and microstructure, as well as the PA effect on J_c , should be investigated.

In the present study, tapes after two-step heat treatment were post-annealed (PA) with different parameters. The phase

✉ Shengnan Zhang
snzhang@c-nin.com

✉ Pingxiang Zhang
pxzhang@c-nin.com

¹ State Key Laboratory of Solidification Processing, Northwestern Polytechnical University, Xi'an 710072, China

² Northwest Institute for Nonferrous Metal Research (NIN), Xi'an 710016, China

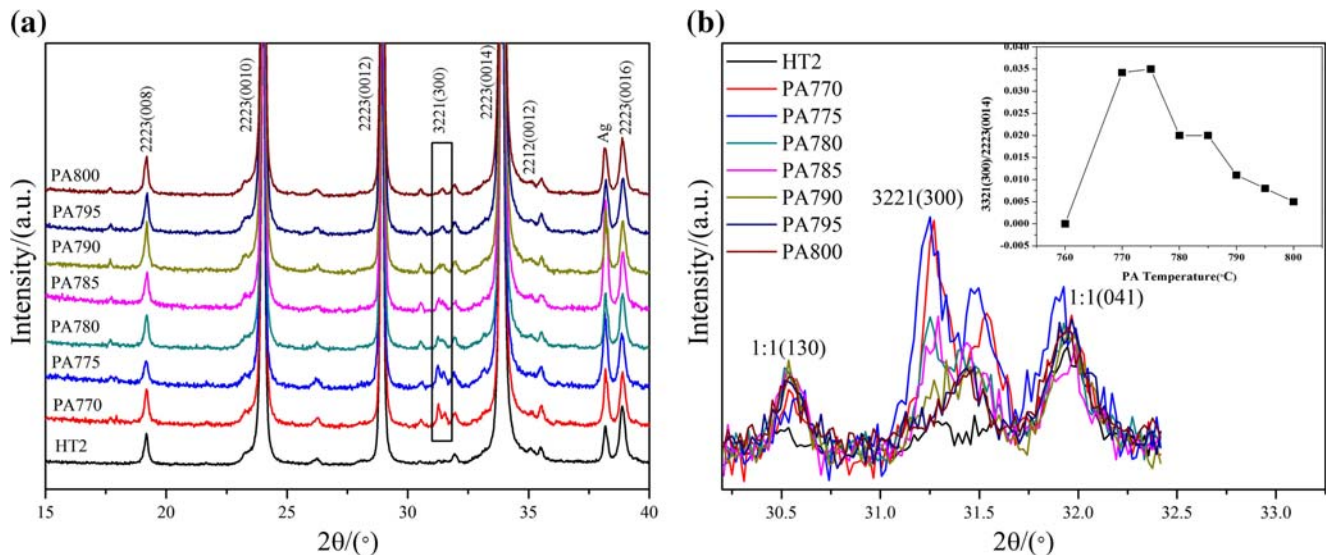


Fig. 1 XRD diffraction patterns of HT2 and PA samples sintered within 770–800 °C. **a** Full scale. **b** Amplifying region of $2\theta = 30.2\text{--}32.7^\circ$

evolution process and current capacity have been studied on the AgAu sheath with different PA process, and the mechanism of the post-annealing is discussed based on the above results.

2 Experiment

The (Bi, Pb)-2223 precursor powders were prepared with a two-powder process [18], with the starting materials of Bi_2O_3 , PbO , SrCO_3 , CaCO_3 , and CuO (> 99.9%). The average composition of the 2223 precursor was $\text{Bi}_{1.76}\text{Pb}_{0.34}\text{Sr}_{1.93}\text{Ca}_{2.02}\text{Cu}_{3.06}\text{O}_x$. 37-filamentary Ag-Au sheathed tapes were prepared by powder in tube (PIT) technique. Samples of as-rolled tapes with the length of 15 cm were sintered at 826 °C for 15 h in 7.5% O_2 (HT1), and then after, tapes were rolled to be 0.25 mm in thickness; the tapes were sintered at 826 °C for 78 h in 7.5% O_2 (HT2), with the sample called HT2 sample. The HT2 samples were post-annealed with the PA temperature between 770 and 800 °C for 36 h; corresponding samples were named as PA770, PA775, PA780, PA785, PA790, PA795, and PA800, respectively.

The phase composition in the tapes was determined using X-ray diffraction. The volume fractions of Bi-2223 and Bi-

2212 phase can be calculated from the intensity I of some selected peaks by the following relation:

$$V_{2223}(\%) = I_{2223(0010)} / [I_{2223(0010)} + I_{2212(008)}] \times 100\% \quad (1)$$

$$V_{2212}(\%) = I_{2212(008)} / [I_{2223(0010)} + I_{2212(008)}] \times 100\% \quad (2)$$

where $I_{2223(0010)}$ and $I_{2212(008)}$ are the intensities of (0010) peak of Bi-2223 and (008) peak of Bi-2212, respectively. The existence status of Pb element in Bi-2223 tapes was performed by X-ray photoelectron spectroscopy (XPS). The microstructures of the sintered tapes were investigated by scanning electron microscopy (SEM). Critical currents (I_c) were measured using a standard four-probe technique with the criterion of 1 $\mu\text{V}/\text{cm}$. AC susceptibility was measured by the superconducting quantum interference device with the AC magnetic field of 0.5 Oe and frequency of 333 Hz from 60 to 120 K. J_c -B dependence was determined in applied fields parallel and perpendicular to the tape plane direction at 77 K from 0 to 0.6 T, respectively.

3 Results

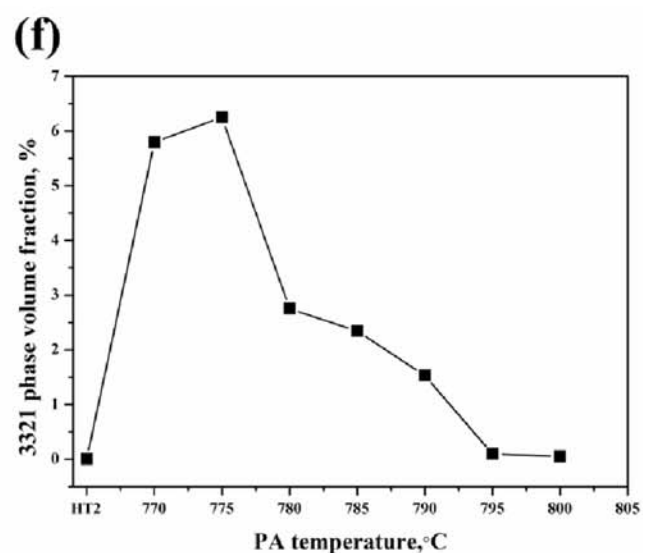
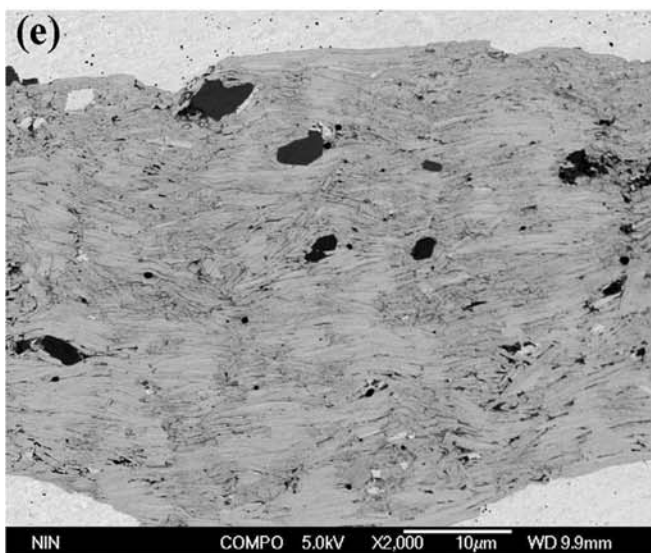
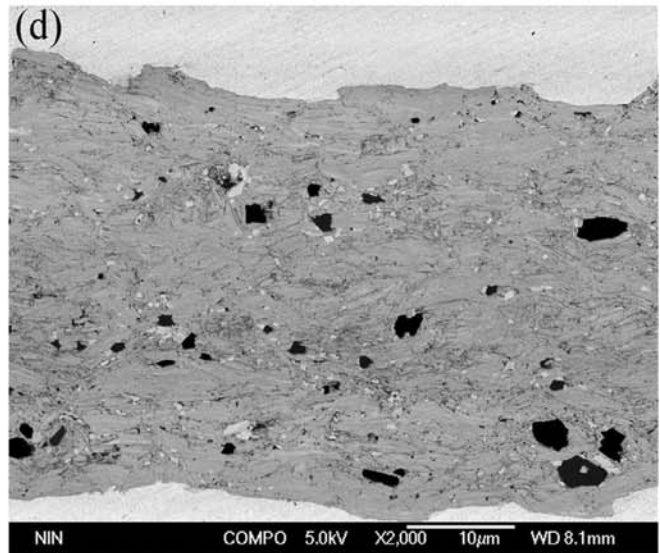
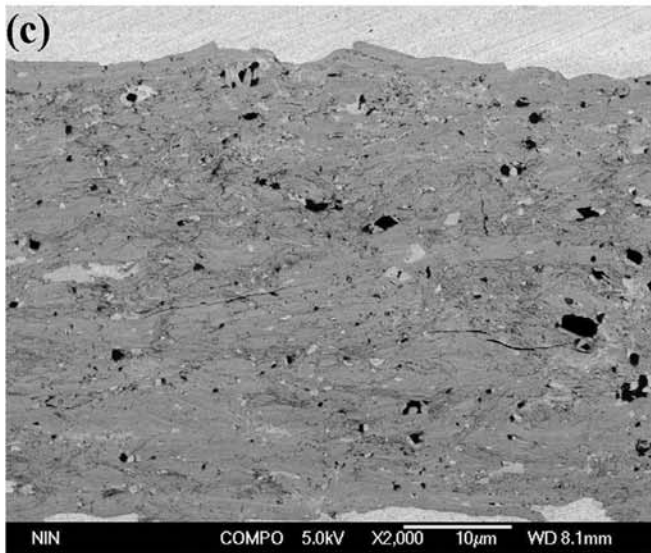
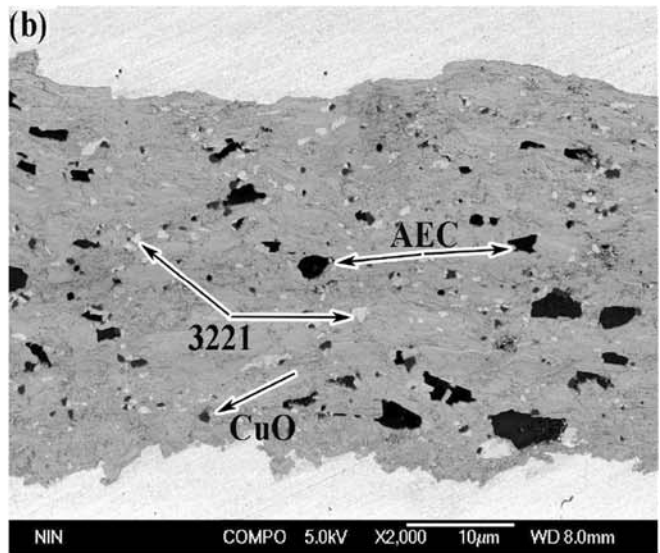
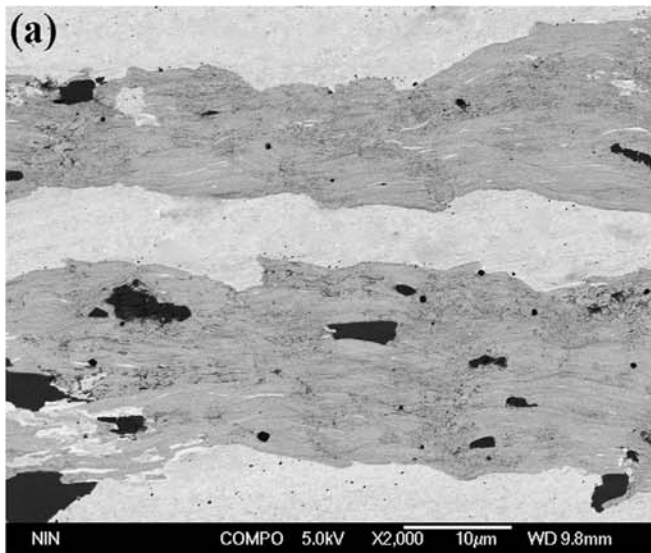
3.1 Phase Composition and Microstructures

X-ray diffraction patterns of Bi-2223 tapes after HT2 and PA process with different post-annealing temperature are shown in Fig. 1a. The existences of secondary phases including

Fig. 2 Backscattered electron images of the cross section of HT2 and PA samples sintered within 770–800 °C. **a** HT2, **b** 770 °C, **c** 780 °C, **d** 790 °C, and **e** 800 °C. The dark gray matrix, the white particles, and the large black particles are Bi-2223, 3221, and alkaline earth cuprate (AEC) phases. **f** PA temperature dependence of 3221 phase volume fraction

Table 1 Microstructural and physical parameters of HT2 and PA samples sintered within 770–800 °C

| PA temperature | HT2 | 770 | 780 | 790 | 800 |
|---|--------|--------|--------|--------|--------|
| 3221(300)/2223(0014) | 0 | 0.0342 | 0.02 | 0.011 | 0.005 |
| Lattice parameter, c , Å | 37.100 | 37.104 | 37.102 | 37.101 | 37.100 |
| Critical temperature, T_c , K | 107.5 | 108 | 108.5 | 108 | 107.5 |
| Peak temperature, T_p , K (@ $H_{ac} = 0.5$ Oe) | 98 | 103 | 105 | 103.5 | 101.5 |



(e)

(f)

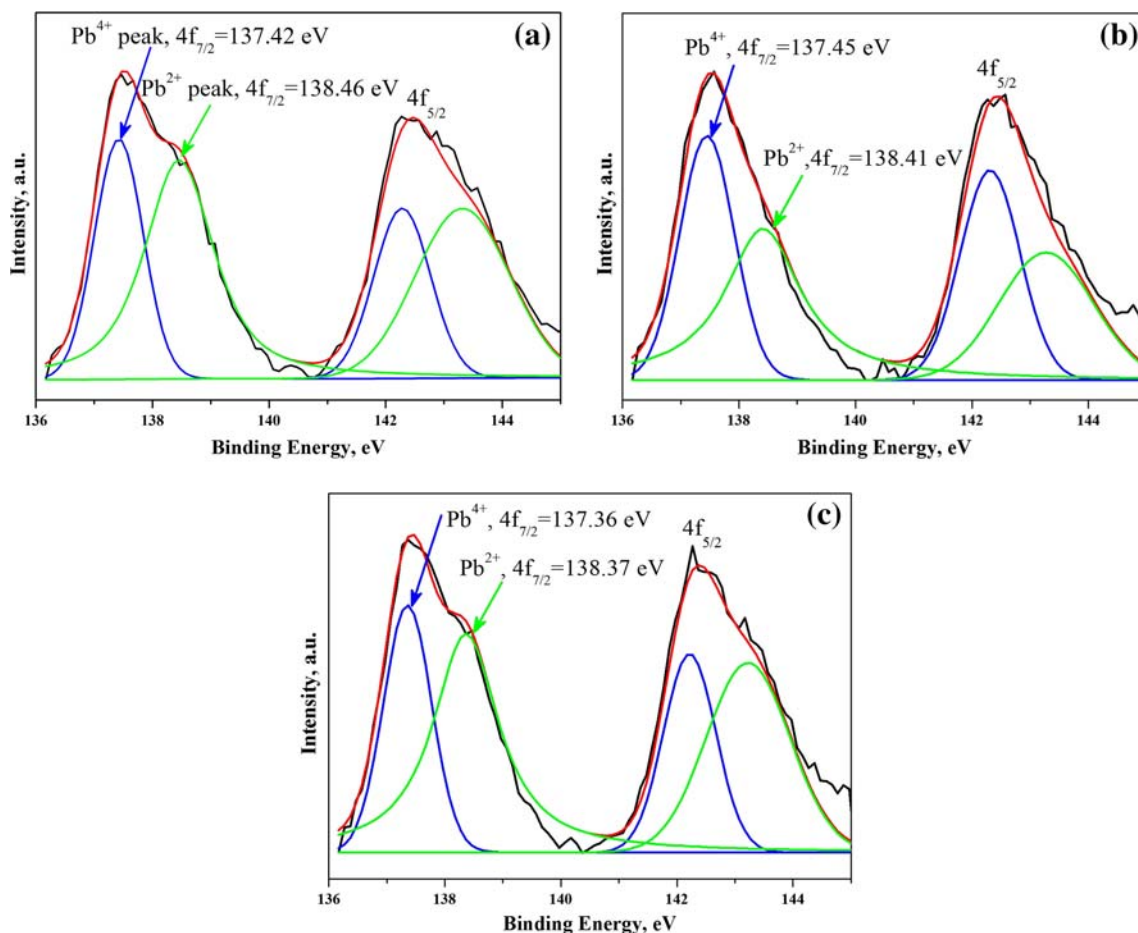


Fig. 3 XPS of Pb ions in Bi-2223 tapes with different PA temperatures. Blue curves represent the Pb^{4+} peaks, and green ones for Pb^{2+} peaks. **a** HT2, **b** 770 °C, and **c** 800 °C

$\text{Bi}_2\text{Sr}_2\text{CaCu}_2\text{O}_{8+\delta}$ (2212) and $(\text{Ca}, \text{Sr})\text{CuO}_2$ (1:1 AEC, alkali earth cuprates) phase can be detected besides Bi-2223 phase as major phase. Based on the calculation by Eqs. (1) and (2), the contents of Bi-2223 phase are approximately 94% in different tapes regardless of the PA temperature, and after post-annealing, the content of Bi-2212 phase slightly decreases. In Fig. 1a, it can be observed that a Pb-rich $(\text{Pb}, \text{Bi})_3\text{Sr}_2\text{Ca}_2\text{CuO}_x$ (3221, $2\theta = 31.5^\circ$, 300/111) phase appears after the post-annealing process as circled out based on the JCPDS Card No. 44-0053. There is no 3221 phase in the HT2 sample, which implies that the cooling rate during the furnace cooling process we adopted in HT2 process is not small enough for the formation of 3221 phase [19]. In Fig. 1b, the intensity ratio between the 3221 (300) peak and Bi-2223 (0014) peak for the tapes with different post-annealing temperatures is plotted in the inset and listed in Table 1. It can be seen that with the increase of PA temperature, the intensity of 3221 (300) peak first increases and then decreases, which suggests that the PA temperature of 770–780 °C is suitable for the precipitation of 3221 phase.

Figure 3 shows the SEM backscattered images of the cross section of tapes after HT2 and different PA temperatures. In all these tapes, the majority phase is Bi-2223 along with small amounts of AEC and CuO phase, shown as black and dark gray particles. In Fig. 2a, there is no white 3221 phase in HT2 sample, which suggests that the 3221 phase begins to appear only during PA process. The volume fraction of 3221 phase is calculated based on the statistics of large amount of SEM images, and the results are shown in Fig. 2f. With the increase of PA temperature, the content of the 3221 phase first increases then decreases. When PA temperature reaches 800 °C, there is nearly no 3221 phase. The changing tendency of 3221 phase content obtained with SEM images analysis is consistent with that obtained with XRD analysis.

Considering that the valence of Pb element is different in (Bi, Pb) -2223 phase and in Pb-rich 3221 phase, it is possible to study the existence status of Pb in Bi-2223 tapes with different PA processes based on the characteristic of XPS. XPS patterns of Pb ions of the HT2, PA770, and PA800 samples are shown in Fig. 3. All the Pb patterns can be fitted into two peaks,

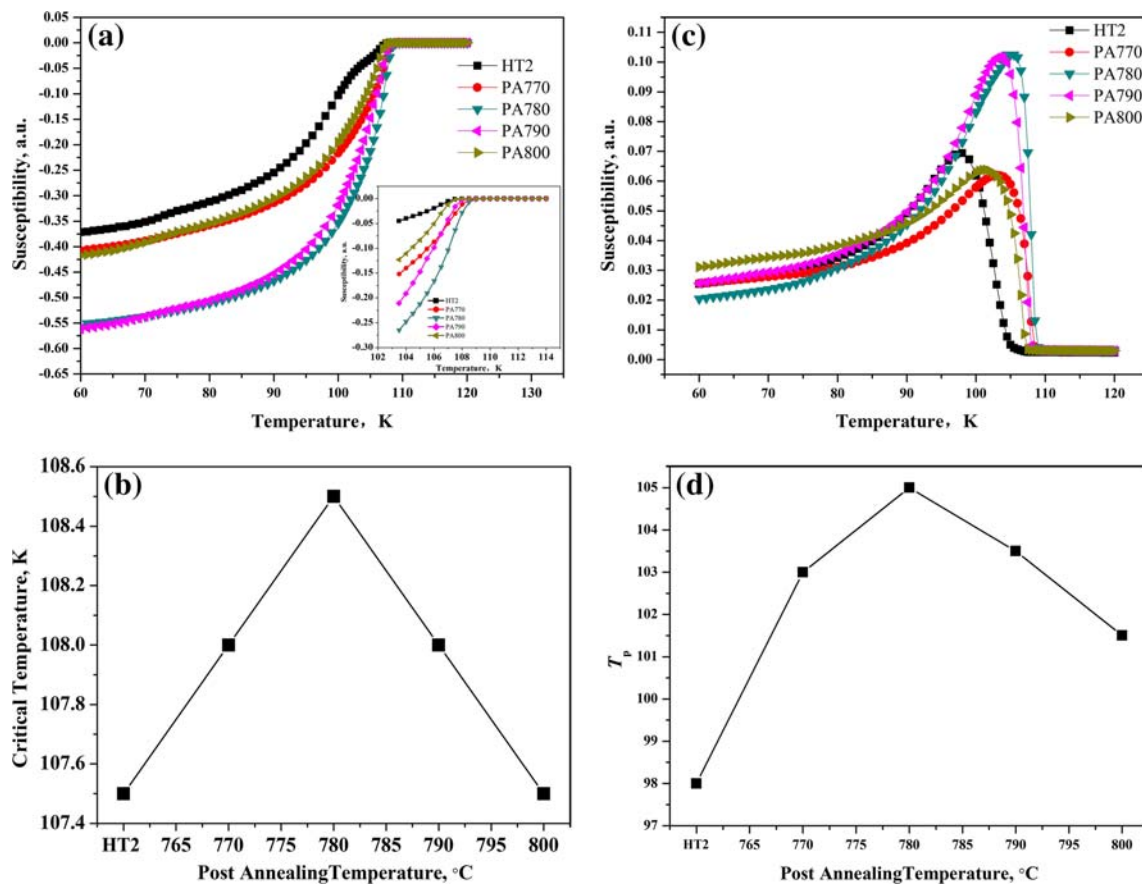


Fig. 4 a PA temperature dependence of the ac susceptibility for HT2 and PA samples sintered within 770–800 °C in the ac field amplitude of 0.5 Oe at the frequency of 333 Hz. The transition areas of the real component χ' were plotted in the inset; the critical temperature values

as a function of PA temperature are shown in **b**; PA temperature dependence of the imaginary component χ'' is shown in **c**; **d** the PA temperature dependence of peak temperature, T_p

suggesting the coexistences of Pb^{2+} and Pb^{4+} ions as marked in Fig. 3. Based on the XPS fitting results, the ratio of $Pb^{4+}:Pb_{total}$ increases from 0.37 for HT2 sample to 0.42 for PA770 sample then decrease to 0.38 for PA800 sample. The higher content of Pb^{4+} ions increases after PA suggests that the Pb^{2+} ions in (Bi,Pb)-2223 phase have been oxidized to Pb^{4+} ions to form Pb-rich phase.

3.2 Superconducting Properties

AC susceptibility is widely used as a nondestructive method for the determination and characterization of the intergrain connections in the polycrystalline high-temperature superconductors [20–23]. The temperature dependencies of the real component, χ' , and imaginary component, χ'' , of AC susceptibility for the HT2, PA770, PA780, PA790, and PA800 samples were measured in an AC field of 0.5 Oe with the frequency of 333 Hz and plotted in Fig. 4a and Fig. 4c, respectively. The transition areas of the real component χ' were plotted in the inset of Fig. 4a. Based on the critical temperature values as a function of PA temperature, which is shown in Fig. 4b, the

onset T_c changes systematically with different PA processes. The T_c value increases from 107.5 K for HT2 sample to 108.5 K for PA780 sample, then decreases to 107.5 K for PA800 sample. For Bi-based superconductors, the superconducting transition temperature T_c is mainly determined by the carrier concentration on [Cu-O₂] layer, which is produced by excess oxygen and a Bi-O bilayer. So the T_c value increases after PA implies the change of oxygen content in Bi-2223 phase.

Correspondingly, on each imaginary component curves, χ'' , a peak appears, which is the measure of dissipation in the sample. Therefore, by examining the change of peak temperature, T_p , on the χ'' curve, the weak link behavior in the superconducting materials can be discussed. As shown in Fig. 4d, the T_p values increase with PA temperature until 780 °C from 98.0 to 105.0 K, then decreases to 101.5 K with further increase of PA temperature. This result suggests that the intergranular connections between grains in the Bi-2223 sample have been greatly improved by a proper amount of 3221 phase precipitation.

The values of J_c at 77 K in the self-field of (Bi,Pb)-2223/AgAu tapes as a function of PA temperature is shown in Fig.

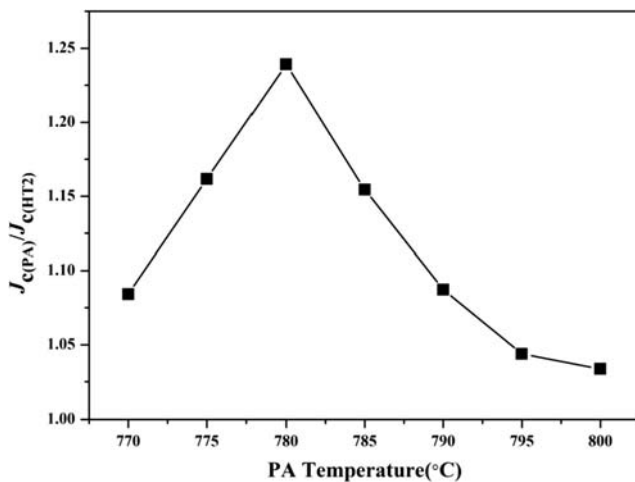


Fig. 5 Temperature dependence of the post-annealing on the critical current density for samples post-annealed in 7.5% O_2 for 36 h

5, where $J_{c(PA)}$ denotes J_c of the PA samples and $J_{c(HT2)}$ denotes J_c of the HT2 sample. It can be observed that within the performed PA temperature range from 770 to 800 °C, all the J_c values have been effectively enhanced after PA, with all the $J_{c(PA)}/J_{c(HT2)}$ values higher than 1. Especially with the post-

annealing at the temperature 780 °C, J_c is improved by 24%. Then, the enhancement of J_c goes down with increasing PA temperature. Therefore, PA at 780 °C can be recognized as the optimized temperature of (Bi,Pb)-2223/AgAu tape. Qu et al. [24] think that the optimum PA temperature of (Bi,Pb)-2223/Ag tape is 790–800 °C. Optimum PA temperature difference is likely caused by low oxygen diffusion rate of AgAu sheath comparing with Ag sheath.

Figure 6 shows the relationship between both the critical current density, J_c (77 K, 1 $\mu V/cm$) values, and normalized J_c values (J/J_{c0}) and the applied field parallel and perpendicular to the tape plane for samples before and after post-annealing. It is clearly observed that J_c of all samples decreases significantly with increasing applied magnetic field, and J_c of PA780 sample reached maximum values in both parallel and perpendicular field. The high normalized J_c value in parallel field shows that the densities of strongly couple grains in PA780 sample are higher than other PA and HT2 samples. The normalized J_c values in perpendicular field of all the samples are nearly the same, which suggests that the flux pinning properties are almost unchanged. So it is the better intergrain connections, which contributes to the enhancement of J_c .

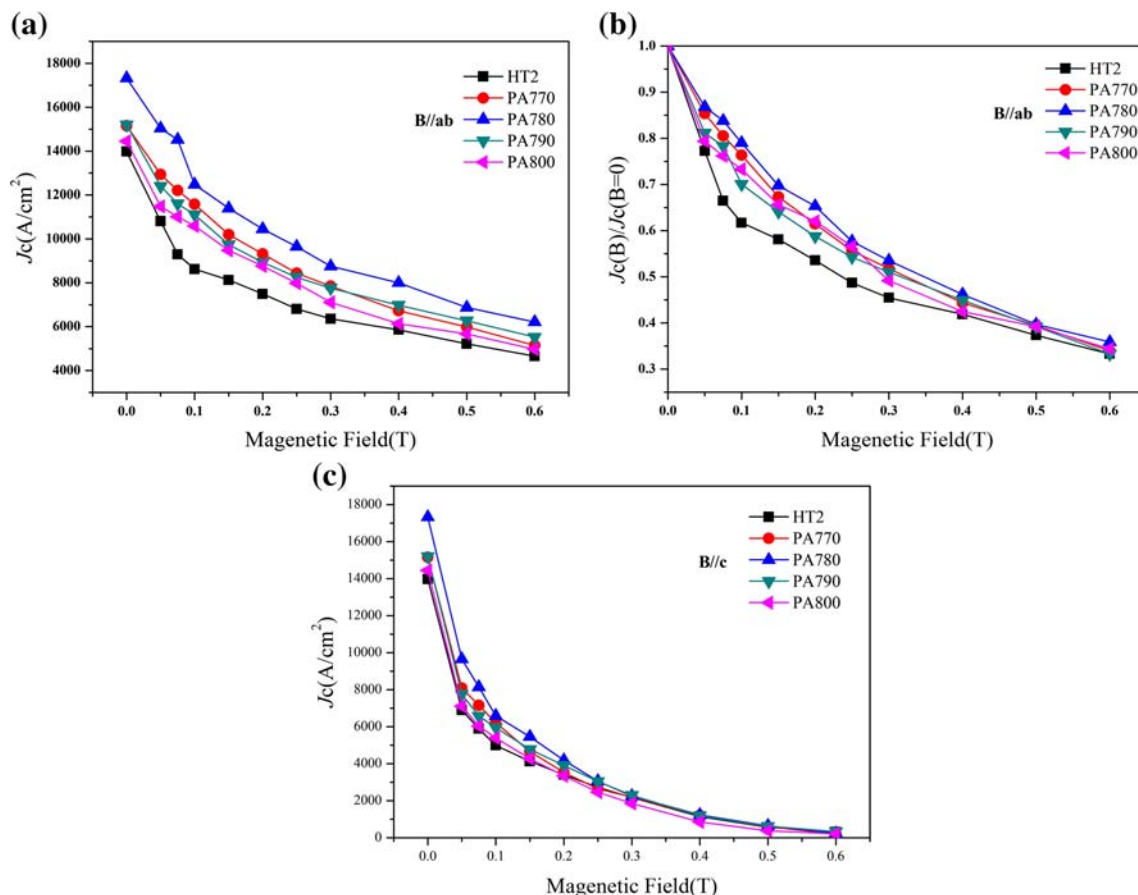


Fig. 6 **a** Critical current density and **b** normalized J_c as a function of magnetic field applied parallel to the ab plane for HT2 and PA samples sintered within 770–800 °C. **c** Critical current density and **d** normalized J_c as a function of perpendicular magnetic field

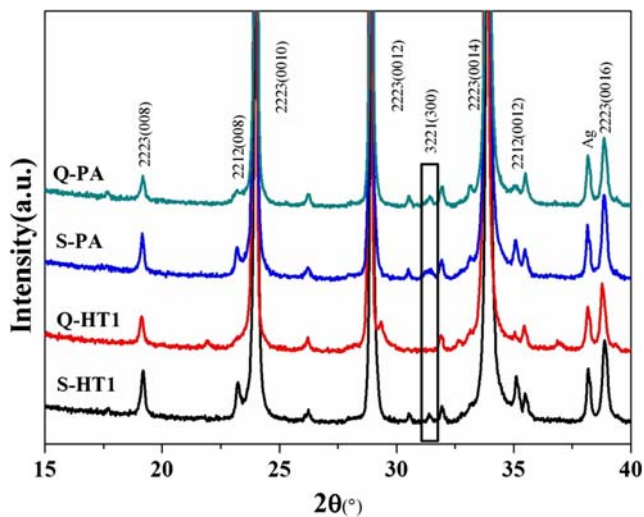


Fig. 7 XRD diffraction patterns of Bi-2223 tapes after HT1 and PA process

4 Discussion

By analyzing these XRD patterns, the origin of 3221 phase can be deduced. Based on previous reports, there are two possible origination of Pb-rich 3221 phase, namely the residual liquid phase [24, 25] and the (Bi, Pb)-2223 [26]. By calculating the lattice parameter c from these XRD patterns, as listed in Table 1, it shows that the variation of c for (Bi, Pb)-2223 phase is within 0.01 Å. Therefore, the Pb content of (Bi, Pb)-2223 changes a little [27]. Thus, it can be deduced that not much Pb has originated from (Bi, Pb)-2223 phase after PA,

suggesting that the (Bi, Pb)-2223 phase cannot be the main Pb source of 3221 phase.

In order to confirm that liquid phase is the major source of Pb for the formation of 3221 phase, samples with different liquid phase contents are obtained. Two as-rolled tapes with the length of 15 cm are thermo-mechanically processed in 7.5% O₂/Ar atmosphere by two heat treatments. In the first heat treatment (HT1) process after sintering under 826 °C for 30 h, the two samples are quenched in air and slow cooled (1 °C/h from 826 to 778 °C and then furnace cooling), respectively, which were named as Q-HT1 and S-HT1 accordingly. Then, the both samples were post-annealed with PA temperature 770 °C for 12 h; these samples were named as Q-PA and S-PA, respectively.

X-ray diffraction patterns of Bi-2223 tapes after HT1 and PA process are shown in Fig. 7. As circled out, 3221 phase appears in the S-HT1 tape, but there is no 3221 phase in the Q-HT1 tape; 3221 phase exists in the both two tapes after PA process. The intensity ratios between the 3221 (300) peak and the Bi-2223 (0014) peak are 0.01139 and 0.02236 for S-PA and Q-PA tapes, respectively; Q-PA tape contains about 96% more 3221 phase than S-PA tape. BSE images of Fig. 8 show the same results as XRD; in addition, some white liquid phase as pointed out appear in the Q-HT1 tape, and then disappear after PA process.

Table 2 shows the I_c values (77 K, 0 T) and Bi-2223 phase contents of Bi-2223 tapes after HT1 and PA process. The Bi-2223 phase content of S-HT1 tape was only 3% higher than Q-HT1 tape, but I_c of S-HT1 tape was 394% higher than Q-HT1 tape. After PA, the Bi-2223 phase content had increased

Fig. 8 Backscattered electron images of the cross section of HT1 and PA samples (a) S-HT1, (b) Q-HT1, (c) S-PA, and (d) Q-PA

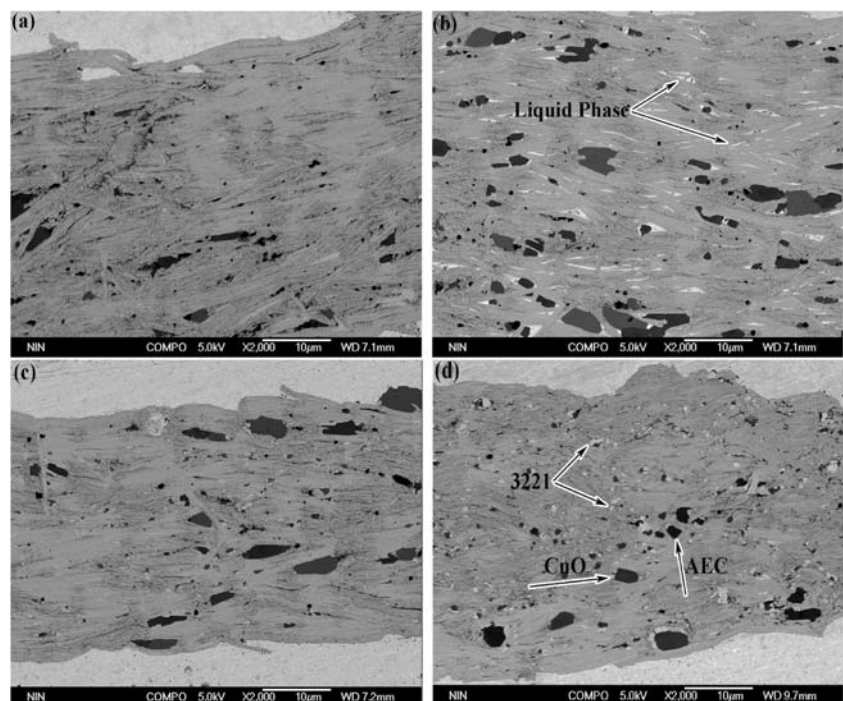


Table 2 Summary of Bi-2223 phase contents and I_c value

| Sample | %2223(I_c) | | I_{c-PA}/I_{c-HT1} |
|--------------|----------------|--------------|----------------------|
| | HT1 | PA | |
| Quenching | 89.5 (5.4A) | 90.6 (57.9A) | 10.7 |
| Slow cooling | 92 (21.3A) | 92.3 (65.9A) | 3.1 |

slightly in both tapes; liquid phase in Q-HT1 tape disappears, whereas I_c increased by about a factor of 11 in Q-PA tape but only by a factor of 3 in S-PA tape. Therefore, it can be confirmed that the increased I_c after PA can be contributed to the reduction of liquid phase from grain boundary of Bi-2223 phase during PA. Considering that the residual liquid phase blocks the current transport, the precipitation of 3221 phase can improve the intergrain connections. The small increase of I_c in S-PA tape compared with Q-PA tape was due to S-HT1 tape having less liquid than Q-HT1 tape. Therefore, it can be deduced that the residual liquid phase is a main source of 3221 phase.

5 Conclusions

In this study, the influences of PA on the phase formation process of $(Pb, Bi)_3Sr_2Ca_2CuO_x$ (3221), microstructures, and the current capacity of AgAu sheathed Bi-2223 tapes and the source of 3221 phase were systematically investigated. Experimental results showed that 3221 phase appeared after PA process with the phase content first increasing then decreasing with increasing PA temperature. The critical temperature T_c and peak temperature (T_p) obtained by AC susceptibility measurement were both increased after PA reached the maximum value at 780 °C simultaneously. Most 3221 phase is thought to form from crystallization of remnant liquid phase during the PA process. The crystallization removes liquid from Bi-2223 grain boundaries after HT1, enhancing the Bi-2223 connectivity. Thus, both the self-field and in-field J_c values (parallel to the ab plane) have been obviously enhanced. The maximum J_c value of 17.3 kA/cm² was obtained when PA temperature reached 780 °C for 37-filamentary Bi-2223/AgAu tapes, which is 24% higher than that of the HT2 sample. Although J_c value of Bi-2223/AgAu tapes is enhanced by PA, which is still ~20% lower than Bi-2223/Ag tapes, the low thermal conductivity makes them one of the best candidates for current leads. Therefore, further optimization is still worthy to do.

Funding Information This study was financially supported National Key Project of Magneto-Constrained Fusion Energy Development Program under Grant No. 2015GB115001, Science and Technology Plan of Weiyang District, Xi'an No. 201904, Key International Cooperation

Project in Shaanxi Province No. 2019KWZ-04, and National Key Research and Development Program No. 2017YFB0902303.

References

- Hayashi, K.: Jpn. J. Appl. Phys. **50**, 080001 (2011)
- Kagiyama, T., Yamazaki, K., Kikuchi, M., Yamade, S., Nakashima, T., Kobayashi, S., Hayashi, K.: IOP Conf. Ser.: Mater. Sci. Eng. **18**, 152001 (2011)
- Osabe, G., Ayai, N., Kikuchi, M., Tatamidani, K., Nakashima, T.: Physica C. **470**, 1365 (2010)
- Nakashima, S., Manabu, S., Inada R., Nakamura Y., Oota, A.: Physica C. 426–431,1149 (2005)
- Lu, X.Y., Watanabe, K., Yi, D., Chen, H., Nagata, A.: Physica C. 471,1090 (2011)
- Shalaby, M.S., Hashem, H.M., Hammad, T.R., Wahab, L.A., Marzouk, K.H., Soltan, S.: J. Radi. Res. Appl. Sci. **9**, 345 (2016)
- Zelati, A., Amirabadzadeh, A., Kompany, A.: J. Supercond. Nov. Magn. **27**, 2185 (2014)
- Matsushita, T., Himeda, Y., Kiuchi, M.: Supercond. Sci. Technol. **19**, 1110 (2006)
- Fujishiro, H., Ikebe, M., Noto, K.: IEEE Trans. Appl. Supercond. **30**, 1645 (1994)
- Yi, H.P., Song, X.H., Liu, L., Liu, R., Kang, W.: Physica C. **426–431**, 1176 (2005)
- Suzuki, T., Yumoto, K., Mamiya, M., Hasegawa, M., Takei, H.: Physica C. **301**, 173 (1998)
- Kim, W.J., Kwon, S.C., Lee, H.G., Hong, G.W., Kuk, H.-I.I.: Supercond. Sci. Technol. **10**, 250 (1998)
- Marti, F., Grasso, G., Grivel, J.C., Flukiger, R.: Supercond. Sci. Technol. **11**, 485 (1998)
- Li, M.Y., Chen, X.P., Qu, T.M., Yi, H.P., Han, Z., Liu, Q.: Physica C. **412–414**, 1091 (2004)
- Jiang, J., Cai, X.Y., Chandler, J.G., Patnaik, S., Polyanskii, A.A., Yuan, Y., Hellstrom, E.E., Larbalestier, D.C.: IEEE T. Appl. Supercon. **13**, 3018 (2003)
- Yuan, Y., Jiang, J., Cai, X.Y., Larbalestier, D.C., Hellstrom, E.E.: Appl. Phys. Lett. **84**, 2127 (2004)
- Kobayashi, S., Yamazaki, K., Kato, T., Ohkura, K., Fujino, K., Fujikami, J., Ueno, E., Ayai, N., Kikuchi, M., Hayashi, K., Sato, K., Hata, R.: Physica C. **426–431**, 1132 (2005)
- Ma, X. B., Zhang, S. N., Yu, Z. M., Liu, G. Q, Li, C. S., Li, J. S., Zhang, P. X.: J. Supercond. Nov. Magn. **32**, 2391 (2019)
- Chen, X.P., Li, M.Y., Qu, T.M., Liu, Q., Han, Z.: Supercond. Sci. Technol. **16**, 1162 (2003)
- Salamati, H., Kameli, P.: Physica C. **403**, 60(2004)
- Gul, I. H., Amin, F., Abbasi, A. Z., Anis-ur-Rehman, M., Maqsood, A.: Physica C. **449**, 139(2006)
- Mihalache, V., Deac, I. G., Pop, A. V., Miu, L.: Current Applied Physics. **11**, 1010(2011)
- Kameli, P., Salamati, H., Eslami, M.: Solid State Commun. **137**, 30(2006)
- Qu, T.M., Han, Z., Flukiger, R.: Physica C. **444**, 71(2006)
- Flukiger, R., Grasso, G., Grivel, J.C., Marti, F., Dhalle, M., Huang, Y.: Supercond. Sci. Tech. **10**, A68 (1997)
- Li, M.Y., Chen, X.P., Qu, T.M., Liu, Q., Han, Z.: Physica C. **411**, 35(2004)
- Jeremie, A., Alami, Y.K., Grivel, J.C., Flukiger, R.: Supercond.Sci. Tech. **6**, 730 (1993)

Publisher's Note Springer Nature remains neutral with regard to jurisdictional claims in published maps and institutional affiliations.